Hot-electron transport for many-valley semiconductors by the method of nonequilibrium statistical operators

M. Liu,* D. Y. Xing,* and C. S. Ting
Department of Physics, University of Houston, Houston, Texas 77004

W. T. Xu
Department of Physics, Beijing Normal University, Beijing, China
(Received 10 March 1987; revised manuscript received 21 August 1987)

The method of the nonequilibrium statistical operator has been generalized to study high-field electron transport in many-valley semiconductors. For steady state, the balance equations for momenta, energies, and populations of the hot electrons in various valleys are derived. Taking n-type silicon as an example, we calculate the drift velocity, electron temperatures and repopulations of both cold and hot valleys as functions of electric field ($1-10^5$ V/cm) at several temperatures between $T=8$ K and $T=300$ K. By applying the electric field parallel to the $\langle 111\rangle$, $\langle 100\rangle$, and $\langle 110\rangle$ crystallographic directions, the anisotropic effect for the drift velocity has been investigated. Furthermore, when considering the transient repopulation effect for a given sample with certain length, a negative-differential-mobility region has been obtained. It is shown that our results are not only in excellent agreement with the results of Monte Carlo method but also quantitatively comparable with experimental data in all temperature ranges.

I. INTRODUCTION

Most important semiconductor materials have many-valley band structures, for example, n-type Ge, Si, and GaAs. Much progress[1-3] has been made in the understanding of nonlinear transport of these systems. But so far, most theoretical approaches to high-field electron transport in many-valley semiconductors have been based on either Monte Carlo simulations[4,5] or on solving the phenomenological Boltzmann equation in relaxation-time approximation.[6-8] The nonequilibrium statistical operator (NSO) method, developed by Zubarev,[9] seems to be a powerful tool to treat the nonequilibrium transport problem analytically. It was previously applied to low-field, warm-electron transport in a single-valley semiconductor.[10] Recently, this method has been reexamined, and extended to study the steady-state hot-carrier transport,[11] as well as to the transient transport in the presence of a strong electric field.[12] In this paper, we generalize the NSO method to the case of a many-valley semiconductor, whose nonlinear transport is very different from that of single-valley model. The carrier-transition between different valleys plays an important role in an applied electric field. Both the anisotropic effect on carrier transport and the Gunn effect[13] in many-valley semiconductors are due to the intervalley scatterings. The former will be discussed in this paper by taking n-type Si with its six equivalent valleys as an example, and the latter has been studied in another paper[14] for GaAs using the Green's function approach. It has been shown[11] that the balance equations obtained from NSO (Ref. 9) and the Green's-function approach[15] are actually identical with each other. As pointed out by us in Ref. 12, the steady-state balance equations used in the practical calculation[11] are in fact semiclassical; the quantum effects are shown to be negligible in the electric field range under our investigation.

One of the main purposes of this paper is to check the validity of the balance-equation approach as compared with the Monte Carlo method. It is well known that the zero-field ($E=0$) resistivity obtained from the balance equation corresponds to the result of the force-force correlation function or the memory-function approach.[16,17] When this method[18] is applied to the electron-phonon interaction in a metal, the resistivity reduces to the well-known Bloch-Grüneisen formula,[19] which has been extensively used in literature to analyze the experimental data for both metals and semiconductors. However, the zero-field resistivity obtained from the force-force correlation has been subjected to criticism[20,21] because it does not agree with that of the current-current correlation function[22] or the Boltzmann equation. Another relevant area of questioning seems to be the difference between the results of these two methods as compared with experimental resistivity data. One of the present authors[23] showed previously that when both methods are applied to a real system like a Si-inversion layer at low temperature, the difference in mobilities is very small, and both of these results are in agreement with the experimental data. In a finite or high electric field ($E\neq 0$), there is no other tractable numerically analytic theory for the nonlinear transport except the phenomenological Boltzmann equation. Whether the balance-equation approach at $E\neq 0$ is still subjected to the same criticism of Refs. 20 and 21 at $E=0$ is an open question and has never been carefully analyzed.

The works of Van Kampen[24] and Horing *et al.*[25] seem to support the finite field balance-equation approach. Since it is conventionally believed that the Monte Carlo method yields the most reasonable result for high-field transport, we shall calculate curves of V_d (the drift velocity) versus E on the basis of balance equations for n-type Si along the ⟨111⟩, ⟨100⟩, and ⟨110⟩ directions from the lattice temperature $T=8$ to 300 K, using the identical set of parameters as those in the Monte Carlo calculation.[4] It is shown that the obtained results are not only in excellent agreement with those of Monte Carlo calculation, but also quantitatively comparable with the experimental data.[4]

In Sec. II the Hamiltonian of a semiconductor with many-valley band structure is described. Intravalley scatterings, intervalley electron-impurity, electron-phonon, and electron-electron interactions are considered. In terms of introducing $3n+1$ thermodynamic variables and their conjugates, the method of NSO is extended to study nonequilibrium transport for a semiconductor with n valleys. A perturbative but useful expression of the NSO is given to proceed to the analytical calculation of nonlinear transport with a many-valley model. In Sec. III we discuss steady-state hot-electron transport and set up $3n$ balance equations for momenta, energies, and carrier numbers of n valleys by using NSO. Some detailed expressions are given in Appendix B. In Sec. IV our formulation is applied to steady-state transport for n-type silicon, and the intravalley acoustic-phonon scattering and six phonon models of intervalley scattering are considered. Numerical results for the ⟨111⟩, ⟨100⟩, and ⟨110⟩ directions of applied electric field in a wide temperature range are reported, and the comparison between theory and experiments is discussed. In Sec. V, the size effect of the sample at low temperature is studied. Considering that the repopulation relaxation time may be very long at low temperature and the steady-state repopulation cannot be established in a small sample at low field, we set up transient evolution equations of carrier numbers in both hot and cold valleys, from which, without any adjustable parameter, the results of microscopic calculation are in reasonable agreement with experiments. Sec. VI contains a summary and discussion of results obtained in this paper.

II. METHOD OF THE NONEQUILIBRIUM STATISTICAL OPERATOR

Let us consider a semiconductor system with n-valley band structure in a strong electric field **E**. The electrons distributed in n valleys of the semiconductor are both accelerated by the applied field and scattered by phonons and impurities, finally forming a steady flow of current, which is called stationary nonequilibrium. The total Hamiltonian of the system may be written as

$$H=\sum_{\alpha=1}^{n} H_\alpha+\sum_{\substack{\alpha,\gamma=1\\(\alpha\neq\gamma)}}^{n} H_{\alpha\gamma}+H_{\rm ph} , \tag{1}$$

$$H_\alpha=H_{e\alpha}+H_{ef\alpha}+H_{el\alpha} . \tag{2}$$

Here H_α denotes the electron Hamiltonian of the αth valley, which is composed of three parts: $H_{e\alpha}$, the free-electron Hamiltonian included the intravalley Coulomb interaction; $H_{ef\alpha}$, the interaction of electrons with a constant uniform external electric field **E** along a given direction; and $H_{el\alpha}$, the intravalley interactions of electrons with phonons and n_i randomly distributed impurities. $H_{\rm ph}$ is the phonon Hamiltonian. The expressions of H_α and $H_{\rm ph}$ are well known,[11] and therefore we omit listing them here. In Eq. (1), $H_{\alpha\gamma}$ is the intervalley scattering term between αth and γth valleys; it can be written as

$$H_{\alpha\gamma}=H_{el}^{\alpha\gamma}+H_{ee}^{\alpha\gamma} , \tag{3}$$

with

$$H_{el}^{\alpha\gamma}=\sum_{k,q,\lambda} M_{\alpha\gamma}(q,\lambda)(b_{q\lambda}+b_{-q\lambda}^{\dagger})c_{\alpha,k+q}^{\dagger}c_{\gamma,k} + \sum_{k,q,a} u_{\alpha\gamma}(q)\exp(i\mathbf{q}\cdot\mathbf{R}_a)c_{\alpha,k+q}^{\dagger}c_{\gamma,k} , \tag{4}$$

and

$$H_{ee}^{\alpha\gamma}=\tfrac{1}{2}\sum_{q} v_c(q)\rho_{\alpha,q}\rho_{\gamma,-q} , \tag{5}$$

where $H_{el}^{\alpha\gamma}$ stands for the intervalley electron-phonon and electron-impurity interactions, and $H_{ee}^{\alpha\gamma}$ is the Coulomb interaction between electrons of the αth and γth valleys. $M_{\alpha\gamma}(q,\lambda)$ is matrix element for intervalley electron-phonon scattering, $u_{\alpha\gamma}(q)$ is the intervalley electron-impurity potential, R_a is the position of the ath impurity, $v_c(q)$ is the intervalley Coulomb potential, and $\rho_{\alpha,q}=\sum_k c_{\alpha,k+q}^{\dagger}c_{\alpha,k}$ is the electron density operator of the αth valley.

In order to apply the method of the nonequilibrium statistical operator[9] (NSO) to the present case, the nonequilibrium macroscopic state of the system as a whole needs to be described by the average values of the following set of operators P_m:

$$\{P_m\}=\left\{\sum_{\alpha=1}^{n} H_{e\alpha},\ \sum_{\alpha=1}^{n} P_{\alpha x},\ \sum_{\alpha=1}^{n} N_\alpha,\ H_{\rm ph}\right\} , \tag{6}$$

where $P_{\alpha x}=\sum_k k_x c_{\alpha,k}^{\dagger}c_{\alpha,k}$ is operator of total momentum of electrons for the αth valley along the direction of electric field, $N_\alpha=\sum_k c_{\alpha,k}^{\dagger}c_{\alpha,k}$ being the corresponding electron number operator. The next step is to introduce a set of time-dependent macroscopic parameters $F_m(t)$ constructed to be the thermodynamic conjugate of the P_m as

$$\{F_m(t)\}=\left\{\sum_{\alpha=1}^{n}\beta_\alpha(t),\ -\sum_{\alpha=1}^{n}\beta_\alpha(t)V_\alpha(t) , - \sum_{\alpha=1}^{n}\beta_\alpha(t)[\mu_\alpha(t)-m_\alpha V_\alpha(t)^2/2],\ \beta\right\} , \tag{7}$$

where β_α, m_α, V_α, and μ_α are the inverse of effective temperature, effective mass, average velocity along the direction of electric field, and nonequilibrium chemical potential of the hot carriers in the αth valley, and β is

the inverse of temperature T of the lattice. Here we exclude $H_{el\alpha}$ and $H_{\alpha\gamma}$ from the dynamical quantities in Eq. (6). The justification of such exclusion has been discussed in Ref. 11 in detail. For a system with n valleys, there will be $3n+1$ parameters for each of the sets $\{P_m\}$ and $\{F_m(t)\}$ according to Eqs. (6) and (7). The situation studied in Refs. 10 and 11 only corresponds to the case of $n=1$.

Following Ref. 9, we can write the nonequilibrium statistical operator in the following form:

$$\rho(t)=\exp\left[-s(t,0)+\int_{-\infty}^{0}dt'e^{\varepsilon t'}\dot{s}(t+t',t')\right], \quad (8)$$

with

$$s(t,0)=\phi+\sum_m F_m(t)P_m , \quad (9)$$

$$\phi=\ln \mathrm{Tr}\left[\exp\left[-\sum_m F_m(t)P_m\right]\right], \quad (10)$$

$$\dot{s}(t,0)=\sum_m \dot{F}_m(t)(P_m-\langle P_m\rangle_l^t)+\sum_m F_m(t)\dot{P}_m , \quad (11)$$

$$\dot{s}(t,t')=\exp(iHt')\dot{s}(t,0)\exp(-iHt') , \quad (12)$$

and

$$\langle P_m\rangle_l^t=\mathrm{Tr}\{P_m\exp[-s(t,0)]\} , \quad (13)$$

which satisfies Liouville's equation in the limit of $\varepsilon\to 0$, and can be used to describe nonequilibrium transport process. In this paper we shall focus our attention on steady-state transport, such that $\dot{F}_m(t)=0$. Equation (11) can then be written as

$$\begin{aligned}\dot{s}(t,0)&=\sum_m F_m\dot{P}_m\\&=\sum_{\alpha=1}^{n}[\beta_\alpha\dot{H}_{e\alpha}-\beta_\alpha V_\alpha\dot{P}_{\alpha x}\\&\quad-\beta_\alpha(\mu_\alpha-m_\alpha V_\alpha^2/2)\dot{N}_\alpha]+\beta\dot{H}_{\mathrm{ph}} , \quad (14)\end{aligned}$$

with

$$\dot{P}_m=-i[P_m,H] . \quad (15)$$

The calculation of $\dot{P}_m$ and $\dot{s}(t,0)$ is standard;[11] their expressions are given in Appendix A. It can be easily seen that $\dot{s}(t,0)$ is of the first order in $H_{\alpha\gamma}$ or $H_{el\alpha}$. Therefore, to obtain the balance equations to second order in the electron-phonon, electron-impurity interactions, or the electron-electron interaction between valleys, we use the following expansion of NSO:

$$\begin{aligned}\rho(t)=\rho_l(t)\Big[1+\int_{-\infty}^{0}dt'\,e^{\varepsilon t'}&\times\int_0^1 d\tau\, e^{-\tau s(t,0)}\\&\times\dot{s}(t+t',t')e^{\tau s(t,0)}\Big] , \quad (16)\end{aligned}$$

where

$$\rho_l(t)=\exp[-s(t,0)] \quad (17)$$

is the quasiequilibrium statistical operator corresponding to the isolated carrier distribution without electron-phonon, electron-impurity, and intervalley Coulomb interactions. We wish to emphasize here that $\rho_l(t)$ is actually defined in the relative or moving system rather than the laboratory system. To make this point clearer, by means of the canonical transformation (Ref. 9, p. 275) we transform $H_{e\alpha}$ to the relative system moving with velocity V_α, where the Hamiltonian of the αth valley is $H'_{e\alpha}$:

$$H'_{e\alpha}=H_{e\alpha}-V_\alpha P_{\alpha x}+N_\alpha m_\alpha V_\alpha^2/2 , \quad (18)$$

such that Eq. (17) can be rewritten as

$$\rho_l(t)=\exp\left[-\phi-\sum_{\alpha=1}^{n}\beta_\alpha(H'_{e\alpha}-\mu_\alpha N_\alpha)-\beta H_{\mathrm{ph}}\right], \quad (19)$$

which is just the quasiequilibrium density matrix in the moving systems. Therefore, the average of operator

$$\langle(\cdots)\rangle_l^t=\mathrm{Tr}[(\cdots)\rho_l(t)] \quad (20)$$

should be performed in the moving systems. It is important to notice that the true density matrix is still defined by NSO in Eq. (8). Only from $\rho(t)$ should the correct carrier distribution function in each valley be obtained.

III. BALANCE EQUATIONS FOR MOMENTA, ENERGIES, AND PARTICLE NUMBERS

To construct the balance equations up to second order in $H_{el\alpha}$ and $H_{\alpha\gamma}$, we use the perturbative density matrix of NSO in Eq. (16) to calculate the statistical average of the time derivatives of the operator P_m:

$$\langle\dot{P}_m\rangle^t=\mathrm{Tr}[\dot{P}_m\rho(t)] . \quad (21)$$

Substituting Eqs. (A1)–(A8) into (16) and (21), and using a similar procedure outlined in Ref. 11, after lengthy algebra, we obtain

$$\langle\dot{P}_{\alpha x}\rangle^t=eEN_\alpha+\sum_{\gamma=1}^{n}F_{ei}^{\alpha\gamma}+\sum_{\gamma=1}^{n}F_{ep}^{\alpha\gamma}+\sum_{\substack{\gamma=1\\(\gamma\neq\alpha)}}^{n}F_{ee}^{\alpha\gamma} , \quad (22)$$

$$\langle\dot{H}_{e\alpha}\rangle^t=eEN_\alpha V_\alpha-\sum_{\gamma=1}^{n}W_{ep}^{\alpha\gamma}-\sum_{\substack{\gamma=1\\(\gamma\neq\alpha)}}^{n}W_{ee}^{\alpha\gamma} , \quad (23)$$

$$\langle\dot{N}_\alpha\rangle^t=\sum_{\substack{\gamma=1\\(\gamma\neq\alpha)}}^{n}N_{ep}^{\alpha\gamma} , \quad (24)$$

$$\langle\dot{H}_{\mathrm{ph}}\rangle^t=\sum_{\gamma=1}^{n}\sum_{\alpha=1}^{n}W_{ep}^{\alpha\gamma} , \quad (25)$$

where $F^{\alpha\gamma}$, $W^{\alpha\gamma}$, and $N^{\alpha\gamma}$ are functions of V_α, V_γ, T_α, T_γ, μ_α, and μ_γ; their expressions are given in Appendix B. It can be easily shown that

$$\sum_{\substack{\alpha,\gamma=1\\(\alpha\neq\gamma)}}^{n}W_{ee}^{\alpha\gamma}=0 , \quad (26)$$

$$\sum_{\substack{\alpha,\gamma=1\\(\alpha\neq\gamma)}}^{n}N_{ep}^{\alpha\gamma}=0 , \quad (27)$$

so that

$$\sum_{\alpha=1}^{n} \langle \dot{H}_{e\alpha} \rangle^t + \langle \dot{H}_{\rm ph} \rangle^t = eE \sum_{\alpha} N_\alpha V_\alpha \ , \tag{28}$$

and

$$\sum_{\alpha=1}^{n} \langle \dot{N}_\alpha \rangle^t = 0 \ , \tag{29}$$

which correspond the conservations of energy and carrier number of the whole system.

In steady state (stationary nonequilibrium), the time derivatives of the variables $\langle P_{\alpha x} \rangle^t$, $\langle H_{e\alpha} \rangle^t$, and $\langle N_\alpha \rangle^t$ should vanish. So we have $3n$ balance equations:

$$\langle \dot{P}_{\alpha x} \rangle^t = 0 \ , \tag{30}$$

$$\langle \dot{H}_{e\alpha} \rangle^t = 0 \ , \tag{31}$$

and

$$\langle \dot{N}_\alpha \rangle^t = 0 \ , \tag{32}$$

with $\alpha = 1,2,\ldots,n$. They form a complete set of equations to determine the $3n$ steady-state values of V_α, T_α, and N_α at a given electric field $\mathbf{E}$ and lattice temperature T. The chemical potential μ_α ($\alpha = 1,2,\ldots,n$) of n valleys, which appear in those functions of Eqs. (22)–(24), are determined by the following relation:

$$\langle N_\alpha \rangle_l^t = \sum_k 1/\{\exp[\beta_\alpha(\varepsilon'_{\alpha k} - \mu_\alpha)] + 1\} \ , \tag{33}$$

where $\varepsilon'_{\alpha k}$ is the single electron energy of the αth valley in the moving system with the velocity V_α. $\langle N_\alpha \rangle_l^t = {\rm Tr}[c^\dagger_{\alpha,k} c_{\alpha,k} \rho_l(t)]$ is the local equilibrium distribution function. Finally, the total drift velocity V_d can be obtained:

$$V_d = \sum_{\alpha=1}^{n} n_\alpha V_\alpha \ , \tag{34}$$

with $n_\alpha = \langle N_\alpha \rangle_l^t / N$, and N as the total carrier number. Here we wish to emphasize again that the experimentally measured distribution function for the αth valley should be ${\rm Tr}[c_{\alpha,k} c_{\alpha,k} \rho(t)]$, and $\rho(t)$ is given by Eq. (8).

Recently the authors and collaborators[14] applied the Green's function approach to obtain the transport balance equations of a semiconductor system including two types of valleys. By means of the transformation relation

$$\langle \dot{H}'_{e\alpha} \rangle = \langle \dot{H}_{e\alpha} \rangle^t - V_\alpha \langle \dot{P}_{\alpha x} \rangle^t + (m_\alpha V_\alpha^2/2) \langle \dot{N}_\alpha \rangle^t \ , \tag{35}$$

it can be easily shown that the present result for $n=2$ reduces to that of the Green's function approach,[14] except that the intervalley impurity scattering is not considered in Ref. 14. Recently, we have shown the equivalency between these two methods for a single-valley semiconductor.

In next section we apply our formulas to study the hot-electron transport for n-type Si with six equivalent valleys.

VI. APPLICATION TO n-TYPE Si

For n-type Si, the electrons which contribute to transport are those in the six equivalent valleys which are around the six minima of the conduction band along the $\langle 100 \rangle$ directions. With each valley, the constant energy surface is near an ellipsoid, and the relationship between the energy ε_α and the wave vector $\mathbf{k}$ may be written as

$$\varepsilon_\alpha = \frac{1}{2} \left[\frac{(\mathbf{k}-\mathbf{k}_{0\alpha})_l^2}{m_l} + \frac{(\mathbf{k}-\mathbf{k}_{0\alpha})_t^2}{m_t} \right] , \tag{36}$$

where $1/m_l$ and $1/m_t$ are the longitudinal and transverse components of the inverse effective-mass tensor, respectively, and $\mathbf{k}_{0\alpha}$ indicates the position in the Brillouin zone of the center of the αth valley. The effective mass of the electrons in an ellipsoid valley is anisotropic, and its inverse for a given direction is determined by

$$(1/m)_{\alpha\mathbf{k}} = \frac{\partial^2 \varepsilon_\alpha}{\partial \mathbf{k}^2} \ . \tag{37}$$

For an applied electric field, the conductivity effective mass m^* for the αth valley depends on the angle between its major axis and the direction of the applied field. For an applied field oriented along the $\langle 100 \rangle$ crystallographic direction, the m^* of the carriers in the two valleys whose major axes are along $\langle 100 \rangle$ is m_l, and that of the other four valleys is m_t. For the electric field applied parallel to the $\langle 110 \rangle$ axis, the m^* of two valleys, whose major axes are along $\langle 001 \rangle$, is m_t; that of the other four valleys is $2(1/m_t + 1/m_l)^{-1}$. When the applied field is $\langle 111 \rangle$ oriented, it is a special case that the m^* of six valleys has the same value, $3(2/m_t + 1/m_l)^{-1}$. Since the effective masses of various valleys may be different except for the $\langle 111 \rangle$ applied field, electrons are heated by the electric field $\mathbf{E}$ at a different rate. So in the valleys (hot valleys) whose effective masses are smaller, the electron temperature is higher than in the other valleys (cold valleys). The transfer rate of carriers from hot valleys to cool valleys is larger than in the reverse direction. Therefore the equilibrium population of a hot valley is smaller than that of a cool valley. This is the well-known valley repopulation effect, which results the anisotropy of the drift velocity in many-valley semiconductors.

By performing the Herring-Vogt transformation,[26] the energy–wave-vector relationship in each valley of n-type Si becomes of a spherical type:

$$\varepsilon_\alpha = (\mathbf{k}_\alpha^*)^2 / 2m_0 \ , \tag{38}$$

where $\alpha = 1,2,\ldots,n$, $\mathbf{k}_\alpha^*$ is the transformed wave vector of the αth valley, and m_0 is the mass of the free electron. After this transformation, it is straightforward to apply the method of NSO and balance equations to the semiconductor system with ellipsoid constant energy surface. One needs to note that, while the density-of-state effective mass is $m_D = (m_t^2 m_l)^{1/3}$, the conductivity effective mass m^* depends on the direction of the applied field.

The scattering mechanisms which have been con-

sidered in our method may include acoustic- and optic-phonon intravalley scattering, the intravalley scattering due to ionized or neutral impurities, electron-phonon intervalley scattering (acoustic and optic), and electron-electron interaction. But for high pure n-type Si, the main contribution for carrier transport comes from phonon-assisted transitions: acoustic intravalley scattering, f scattering (between perpendicular valleys) with LA and TO phonons, and g scattering (between parallel valleys) with LO phonons, which are allowed by the selection rules.[27,28] In our numerical calculations, we shall consider three f and three g intervalley scatterings. Their equivalent phonon frequencies $\Omega_{\alpha\gamma}$ and coupling constant $D_{\alpha\gamma}$ are taken from the same values as those in the Monte Carlo calculation.[4] The squared matrix elements of the acoustic intravalley scattering and the intervalley scattering between the αth and γth valleys are

$$M_{\alpha\alpha}(q,\lambda)=E_1^2 q/(2dV_s) \tag{39}$$

and

$$M_{\alpha\gamma}(q,\lambda)=D_{\alpha\gamma}^2/(2d\Omega_{\alpha\gamma}) , \tag{40}$$

respectively. The set of physical parameters used in the present calculations is listed in Table I.[3,4] For comparison, these parameters are entirely identical with those used in the Monte Carlo simulations,[4] and there are no adjustable parameters in our calculation. For a silicon sample with high purity, we expect the carrier concentration N ($<2\times10^{13}$ cm^{-3}) to be small. Even at $T=8$ K, the carrier distribution function is Boltzmann-like. The influence due to both electron-impurity and electron-electron interactions as pointed out by Ref. 4, can be neglected. However their effect may show up only at very low temperatures where the carrier distribution becomes Fermi-Dirac.

Figures 1–4 report the calculated results for a wide temperature range in an electric field applied parallel to different crystallographic directions. In order to display the anisotropic effect, the drift velocities obtained at the different lattice temperatures with the electric field applied parallel to the ⟨111⟩ and ⟨100⟩ axes are shown in Figs. 1(a) and 1(b), together with experimental results. In these figures it is easy to see that the calculated results (solid lines) for the ⟨111⟩ direction are in good agreement with experimental data (solid circles) almost over the entire temperature and electric field ranges. Only at $T=8$ K, for fields below about 10 V/cm, the theoretical values are slightly higher in comparison with experimental ones but are still better than those obtained in the Monte Carlo calculation.[4]

The calculated results (dashed lines) for the ⟨100⟩ direction show a better agreement with experimental data (open circles) at high temperatures ($T>45$ K) than at low temperature ($T<45$ K), and some discrepancies occur as $T<45$ K. However, if one compares our results for the ⟨100⟩ direction with those of the Monte Carlo calculation,[4] one should find that they are in good agreement with each other over the whole temperature range, which supports the reliability of our method since all the parameters used in our calculation are the same as those in the Monte Carlo simulation.[4] The main discrepancy for theoretical results with E parallel to the ⟨100⟩ direction is that they do not reproduce a negative differential mobility (NDM), which is found in experiments at low temperatures and low electric fields. This is because our results are obtained from those steady-state balance equations for momenta, energies, and carrier numbers of the hot and cold valleys. However, at low temperatures and low fields, the effect due to the intervalley electron-phonon interaction is much smaller than that of intravalley electron-phonon interaction. The time duration for the carrier populations in different valleys to reach steady state is very long, and transient repopulation is very important for determining the drift velocity of a small sample. This effect is going to improve greatly the agreement between theory and experiment, which we will discuss in detailed in the next section.

The drift velocities obtained for the ⟨110⟩ direction lie always between those of the ⟨111⟩ and ⟨100⟩ directions over entire temperature and electric field ranges. So only the calculated results (dot-dashed lines) at low temperatures are plotted as in Fig. 1(a); those at high

TABLE I. Set of physical parameters used in the present calculation.

Density	$d=2.329$ g/cm^3
Longitudinal sound velocity	$V_s=9.037\times10^5$ cm/s
Longitudinal effective mass	$m_l=0.9163m_0$
Transverse effective mass	$m_t=0.1905m_0$
Acoustic-deformation-potential parameter	$E_1=9$ eV

	Intervalley scattering	
Type	Equivalent temperature $\Omega_{\alpha\gamma}$ (K)	Coupling constant $D_{\alpha\gamma}$ (eV/cm)
f	210	1.5×10^7
	500	3.4×10^8
	630	4×10^8
g	140	5×10^7
	210	8×10^7
	700	3×10^8

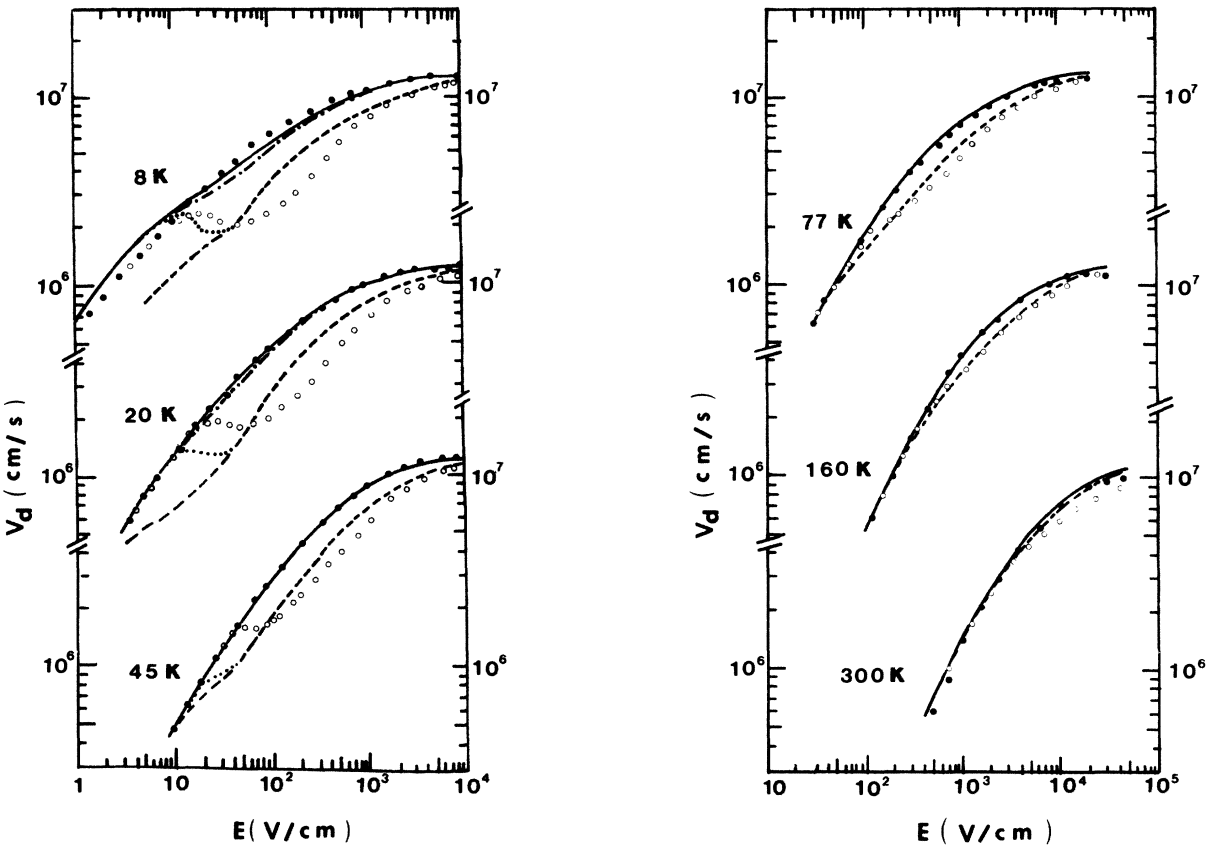

FIG. 1. Electron drift velocity as function of electric field E at the different indicated temperatures. Solid circles and solid lines refer to the experimental and calculated results for the field parallel to ⟨111⟩ directions, respectively. Open circles and dashed lines refer to the experimental and calculated results for the field parallel to ⟨100⟩ directions, respectively. Dot-dashed lines refer to the calculated results for the field parallel to ⟨110⟩ directions at $T=8$ and 20 K. Dotted lines refer to the calculated results considering the transient repopulation effect for the field parallel to ⟨100⟩ directions at lower temperature and lower field, for a sample with length 1050 μm.

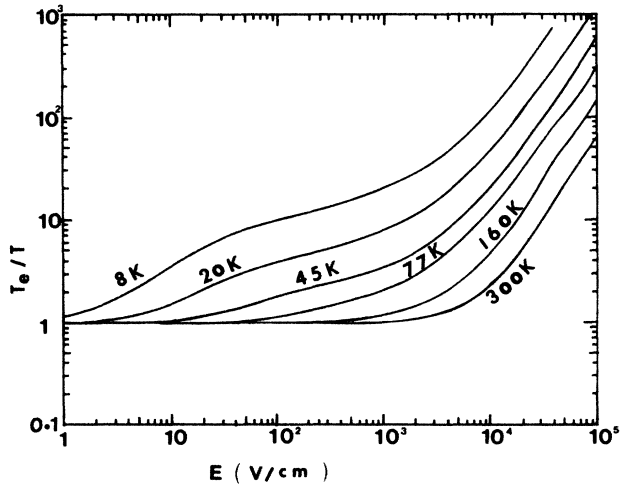

FIG. 2. Temperature ratio T_e/T as a function of electric field E parallel to ⟨111⟩ directions at different indicated temperatures.

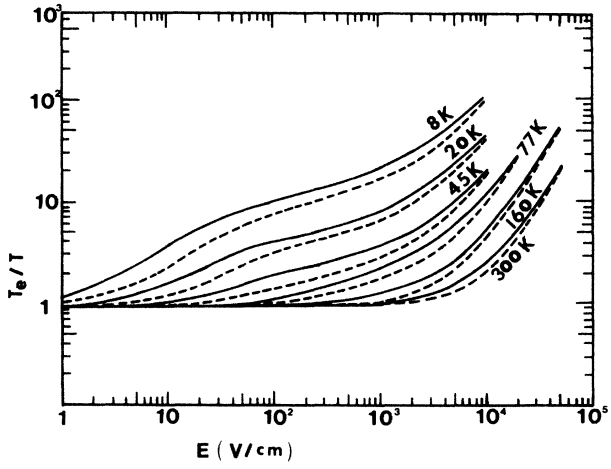

FIG. 3. Temperature ratio T_e/T (solid lines for hot valleys, dashed lines for cold valleys) as a function of electric field E parallel to ⟨100⟩ directions at different indicated temperatures.

temperature are very close to the solid lines with E parallel to the ⟨111⟩ direction and therefore were omitted in the plot. Figures 2 and 3 show the electron effective temperatures as a function of the applied field at different lattice temperatures for the ⟨111⟩ and ⟨100⟩ directions, respectively. For the electric field applied parallel to the ⟨111⟩ axis, since all the six valleys of silicon lie the same symmetrical position, only one effective temperature of electrons needs to be introduced. However, for E along the ⟨100⟩ direction, there are two cold valleys whose major axes are along the direction ⟨100⟩, and four hot valleys whose major axes are perpendicular to ⟨100⟩, so we introduce two electron temperatures T_c and T_h for the cold and the hot valleys, respectively. In Fig. 3, the ratios T_h/T and T_c/T are plotted as solid and dashed curves. The higher the lattice temperature T, the smaller the difference between T_h/T and T_c/T, and at a given temperature T, the ratios T_h/T and T_c/T begin to separate from each other with an increasing electric field, then tend to join together when the field becomes strong. This give a clear explanation of the experimental results that the anisotropic effect increases at decreasing lattice temperature, and it tends to vanish at very low electric fields or very high ones, because the anisotropy of the drift velocity in silicon is due to a repopulation of the hot and cold valleys which depends on the temperature difference between these valleys. The population of a cold valley obtained in the steady-state case is shown in Fig. 4 as a function of field strength (E parallel to the ⟨100⟩ direction) at various temperatures. At each given lattice temperature, there is a peak for the population value of the cold valley at a certain electric field, at which the maximum anisotropic effect in drift velocity occurs. It is easily seen that the population peak of the cold valley lowers and moves towards right as the lattice temperature increases.

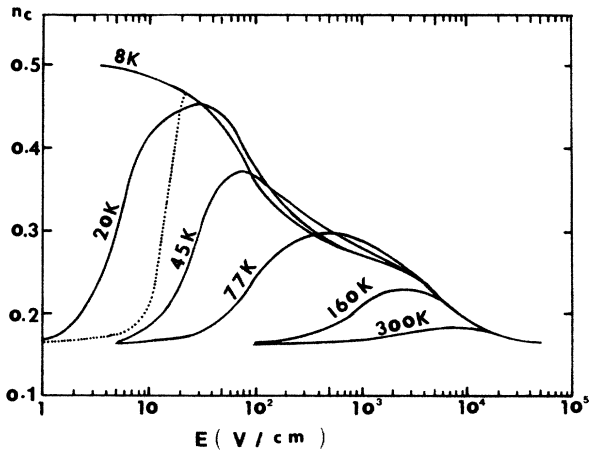

FIG. 4. Population n_c of cold valleys as function of electric field E parallel to ⟨100⟩ directions. The solid lines show the steady-state results at the different indicated temperatures, the dotted line shows the result considering the transient repopulation effect at lower temperature, $T=8$ K, and lower field calculated by a sample with length 1050 μm.

The behavior of the cold valley population at 8 K is unusual. It may be shown that at such a low temperature, the steady-state condition can hardly have been reached in those samples used for drift-velocity measurement.

V. TRANSIENT REPOPULATION EFFECT

In the previous section, the steady-state hot electron transport of n-type Si has been calculated and discussed. A basic assumption there is that the sample length is large enough so that the transit time of electrons across the sample is much longer than their relaxation time, and steady state is established. In many-valley semiconductors there are three types of relaxation time: momentum, energy, and valley repopulation relaxation times. The first two are much shorter than the last one at low temperatures and low electric fields, because the repopulation time depends on the intervalley f transitions (between perpendicular valleys), which require phonons with equivalent temperatures of several hundred K. But at low temperatures and low fields, the average electron energies within both cold and hot valleys are much smaller than the f-phonon energy, and emission processes are also very rare. In such conditions, the repopulation relaxation time is very long, so that the steady-state repopulation cannot be established for small samples used in drift-velocity measurements or calculations. Therefore, we must consider the transient repopulation effect. The drift velocity V_d of electrons is experimentally obtained[4] by measuring the transit time T_R and sample length W and using the simple relationship $V_d=W/T_R$. In our calculation, for a small sample in which the steady-state repopulation cannot be reached, we define a transient drift velocity $V_d(t)$ as

$$V_d(t)=\sum_{\alpha=1}^{n} n_\alpha(t)V_\alpha \ , \tag{41}$$

where $n_\alpha(t)$ is t dependent, and V_α is assumed to reach its intermediate steady-state value. The length of the sample covered in a time T_R is defined as

$$W=\int_0^{T_R} V_d(t)dt \ . \tag{42}$$

In Ref. 4, the transient drift velocity of electrons was obtained by a phenomenological equation in which several parameters were experimentally determined. Here we shall perform an entire microscopic calculation for $V_d(t)$ by Eq. (41), in which $n_\alpha(t)$ can determined in terms of the evolution equation (24) for carrier numbers in both cold or hot valleys:

$$\frac{dn_\alpha}{dt}=\sum_{\substack{\gamma=1 \\ (\gamma\neq\alpha)}}^{n} N_{ep}^{\alpha\gamma}/N \ . \tag{43}$$

This, together with the momentum and energy balance equations, (30) and (31), will construct a complete set of equations to determine V_α, T_α, and transient populations $n_\alpha(t)$. In general, we can solve these nonlinear equations consistently and obtain the numerical values of V_α, T_α, and $n_\alpha(t)$. If we consider a silicon sample of

high purity, the electrons of both hot and cold valleys in quasiequilibrium obey the Maxwell-Boltzmann distribution even at low temperatures. In such cases, for an applied field along a ⟨100⟩ direction, Eq. (43) reduces to a linear differential equation for the population of a cold or a hot valley

$$\frac{dn_c}{dt} = -(n_c - n_{c\infty})/\tau \ , \tag{44}$$

with

$$2n_c + 4n_h = 1 \ ,$$

where n_c and n_h are the fractions of the electrons in a cold and a hot valley, respectively, and $n_{c\infty}$ corresponds to the steady-state fraction of a cold valley in a given field. The physical meaning of τ is clear—it is the repopulation relaxation time. The solution of Eq. (44) is

$$n_c(t) = \tfrac{1}{6}\exp(-t/\tau) - n_{c\infty}[\exp(-t/\tau) - 1] \ , \tag{45}$$

which satisfies the conditions that $n_c(t=0) = \frac{1}{6}$ and $n_c(t \to \infty) = n_{c\infty}$. The expressions of $1/\tau$ and $n_{c\infty}$ are given in Appendix C. The repopulation relaxation time τ is shown as a function of field strength in Fig. 5 (solid curve) together with the experimental data (solid circles) and Monte Carlo results (dashed curve). $n_{c\infty}$, the value of the steady-state repopulation of a cold valley, has been given in Fig. 4. Since at low temperatures and low fields the effect due to f scattering is very small and can be neglected, and the carrier distribution function used in the present calculations is assumed to be a Boltzmann distribution, the balance equations which determined V_α and T_α are independent of the carrier populations of various valleys. From Eqs. (41), (42), and (45) we can obtain $n_c(t)$, $V_d(t)$, and T_R for a given sample with length W. The dotted line in Fig. 4 shows $n_c(t = T_R)$ as a function of field strength at $T=8$ K when $W=1050$ μm is used in drift-velocity calculations.[4] From that result it is easily seen that at low electric fields ($E < 10$ V/cm), $n_c(t = T_R) \simeq \frac{1}{6}$, there is little difference between the populations of the hot and cold valleys, so that there is little anisotropic effect for the drift velocity. In Fig. 1(a), the drift velocity, obtained by the relationship $V_d = W/T_R$ with $W=1050$ μm, is reported as dotted curves at several low temperatures. It shows that, after considering the transient repopulation effect, a negative-differential-mobility (NDM) region was obtained for $T < 45$ K and with an electric field along the ⟨100⟩ direction. This is consistent with the experimental data. Unlike the phenomenological calculation in Ref. 4, our transient calculation is entirely microscopic and without any adjustable parameter. Furthermore, our results agree quantitatively with experimental data for several samples with different lengths at $T=8$ K, which is reported in Fig. 6. We believe that a better agreement with experimental results at low temperature could be obtained when the effects due to electron-impurity and electron-electron interactions are properly considered.

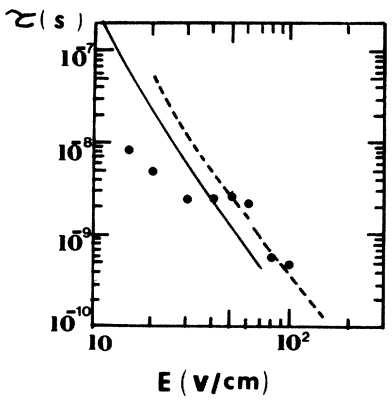

FIG. 5. Repopulation relaxation time as function of electric field parallel to ⟨100⟩ directions at $T=8$ K. Solid circles refer to experimental data, the dashed line refers to the result of Monte Carlo calculation, and the solid line refers to our results.

VI. CONCLUSION

In this paper we have studied the hot electron transport for many-valley semiconductors in a strong and uniform electric field. A set of analytic balance equations, used to determine drift velocities, effective temperatures, and populations of various valleys, is derived from the approach of the nonequilibrium statistical operator. One advantage of this method, which differs from the Monte Carlo simulation and relaxation-time approach, is that

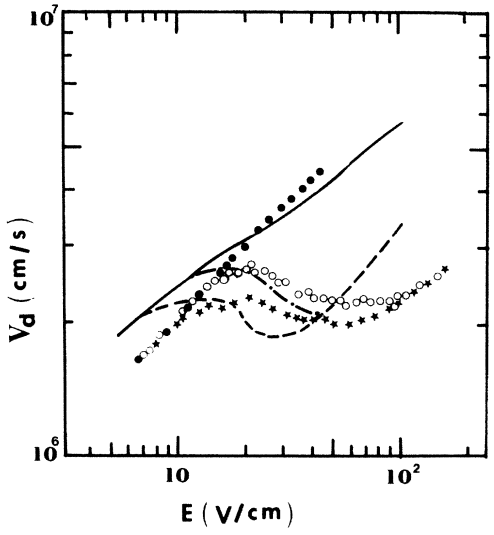

FIG. 6. Electron drift velocity as function of electric field parallel to ⟨100⟩ directions for different sample lengths at $T=8$ K. Stars and open circles refer to experimental results obtained with sample lengths 1050 and 280 μm, respectively; dashed and dot-dashed lines refer to the calculated results obtained with sample lengths 1050 and 280 μm, respectively. For comparison, solid circles and solid lines refer to experimental data and calculated results for the field parallel to ⟨111⟩ directions.

all the average values of the relevant operators and correlation functions are derived microscopically and quantum mechanically by means of the nonequilibrium density-matrix approach. Every term in those balance equations has explicit analytic expressions which can be easily used for numerical computation on a Micro-*VAX* II computer. In the present numerical calculations, the intravalley and intervalley electron-electron interactions are neglected so that the balance equations reduce to the semiclassical ones. However, in our formulation these Coulomb interaction effects have been included in terms of the electron density-density correlation functions. When the density-density correlation functions are evaluated beyond the random-phase approximation (RPA), the obtained balance equations should be superior to the semiclassical ones.[29] One advantage of the present formulation is that the electron-electron interaction effects are included in a natural and consistent way. It is straightforward to extend the present method to study the transient hot-electron transport[12] for many-valley semiconductors. In this paper we have only discussed the transient repopulation effect for a small sample of silicon at low temperatures and low fields. In the present method the valleys of electrons are assumed anisotropic but parabolic, and some additional effects, such as nonparabolicity and complicated device geometries, are not considered. These effects may be important in some situations. How to extend the present theory to account for these effects is currently under investigation.

We have presented our theoretical results for n-type silicon with six equivalent valleys. By applying the electric field parallel to the $\langle 111\rangle$, $\langle 100\rangle$, and $\langle 110\rangle$ directions, it is shown that the anisotropic effect for the drift velocity depends on the lattice temperature and the field strength. The effective electron temperatures and repopulation for both cold and hot valleys have been presented to interpret this anisotropic effect. When the transient repopulation effect is considered, a negative-differential-mobility region has been obtained. Using the identical set of parameters as those in Monte Carlo simulation,[4] it is shown that our results are not only in excellent agreement with those of Monte Carlo method in wide temperature and electric field ranges but also quantitatively comparable with experimental data. Thus we believe that the balance equations obtained from the NSO or Green's-function approach should be considered as a useful tool to deal with hot-electron transport problems in a uniform electric field.

APPENDIX A: THE EXPRESSIONS OF $\dot{P}_m$ AND $\dot{s}(t,0)$

By means of the quantum equation (15), the time derivatives of the operators P_m are obtained as follows:

$$\dot{P}_{\alpha x}=eEN_\alpha - i\sum_{\gamma\neq\alpha}\sum_q \nu_c(q)q_x\rho_{\alpha,q}\rho_{\gamma,-q} - \left[i\sum_{\gamma=1}^{n}\sum_{q,k}(k_x+q_x)R_{\alpha\gamma}(q,k)+\text{H.c.}\right], \tag{A1}$$

$$\dot{H}_{e\alpha}=eEP_{\alpha x}/m_\alpha - i\sum_{\gamma\neq\alpha}\sum_{q,k}\nu_c(q)(\varepsilon_{\alpha,k+q}-\varepsilon_{\alpha k}) \times c^\dagger_{\alpha,k+q}c_{\alpha,k}\rho_{\gamma,-q} - \left[i\sum_{\gamma=1}^{n}\sum_{q,k}\varepsilon_{\alpha,k+q}R_{\alpha\gamma}(q,k)+\text{H.c.}\right], \tag{A2}$$

$$\dot{N}_\alpha=-i\sum_{\gamma=1}^{n}\sum_{q,k}R_{\alpha\gamma}(q,k)+\text{H.c.}\,, \tag{A3}$$

$$\dot{H}_{\text{ph}}=i\sum_{\alpha,\gamma=1}^{n}\sum_{k,q,\lambda}\Omega_{q\lambda}M_{\alpha\gamma}(q,\lambda)(b_{q\lambda}-b^\dagger_{-q\lambda})c^\dagger_{\alpha,k+q}c_{\gamma,k}\,, \tag{A4}$$

with

$$R_{\alpha\gamma}(q,k)=\sum_a u_{\alpha\gamma}(q)e^{i\mathbf{q}\cdot\mathbf{R}_a}c^\dagger_{\alpha,k+q}c_{\gamma,\kappa} + \sum_\lambda M_{\alpha\gamma}(q,\lambda)(b_{q\lambda}+b^\dagger_{-q\lambda})c^\dagger_{\alpha,k+q}c_{\gamma,k}\,, \tag{A5}$$

where m_α is the conductivity effective mass, along the direction of the applied field $\mathbf{E}$, of electrons in the αth valley. H.c. stands for the conjugate term. The summations over γ from 1 to n in Eqs. (A1)–(A5) include both $\gamma=\alpha$ and $\gamma\neq\alpha$; the former corresponds to the contribution of the intravalley scattering, and the latter comes from the intervalley scattering due to phonons and impurities. It can be easily shown that the term $\gamma=\alpha$ in Eqs. (A1), (A2), and (A4) may reduce the same result in a single-valley model [see Eq. (22) of Ref. 11]. Substituting Eqs. (A1)–(A5) into (14), we obtain the expression of $\dot{s}(t,0)$ as

$$\begin{aligned}\dot{s}(t,0)=&-i\sum_{\alpha,\gamma=1}^{n}\sum_{k,q,a}u_{\alpha\gamma}(q)e^{i\mathbf{q}\cdot\mathbf{R}_a}[\beta_\alpha(t)\xi_{\alpha,k+q}-\beta_\gamma(t)\xi_{\gamma k}]c^\dagger_{\alpha,k+q}c_{\gamma,k}\\ &-i\sum_{\alpha,\gamma=1}^{n}\sum_{k,q,\lambda}M_{\alpha\gamma}(q,\lambda)[\beta_\alpha(t)\xi_{\alpha,k+q}-\beta_\gamma(t)\xi_{\gamma k}-\beta\Omega_{q\lambda}]b_{q\lambda}c^\dagger_{\alpha,k+q}c_{\gamma,k}\\ &-i\sum_{\alpha,\gamma=1}^{n}\sum_{k,q,\lambda}M_{\alpha\gamma}(q,\lambda)[\beta_\alpha(t)\xi_{\alpha,k+q}-\beta_\gamma(t)\xi_{\gamma k}+\beta\Omega_{q\lambda}]b^\dagger_{-q\lambda}c^\dagger_{\alpha,k+q}c_{\gamma,k}\\ &-i\sum_{\alpha<\gamma}^{n}\sum_{k,q,k'}\nu_c(q)[\beta_\alpha(t)(\xi_{\alpha,k+q}-\xi_{\alpha k})-\beta_\gamma(t)(\xi_{\gamma,k'-q}-\xi_{\gamma,k'})]c^\dagger_{\alpha,k+q}c_{\alpha,k}c^\dagger_{\gamma,k'-q}c_{\gamma,k'}\,,\end{aligned} \tag{A6}$$

with

$$\xi_{\alpha k}=\varepsilon'_{\alpha k}-\mu_\alpha \ , \tag{A7}$$

$$\varepsilon'_{\alpha k}=\varepsilon_{\alpha k}-k_x V_\alpha+m_\alpha V_\alpha^2/2 \ , \tag{A8}$$

where $\varepsilon'_{\alpha k}$ is the one-electron energy of the αth valley in the moving system with velocity V_α, and $\varepsilon_{\alpha k}$ is that in the laboratory system. They are connected through Eq. (A8).

APPENDIX B: THE EXPRESSIONS OF SEVERAL FUNCTIONS IN THE BALANCE EQUATIONS

The expressions of F_{ei}, F_{ep}, W_{ep}, and N_{ep} in Eqs. (22)–(25) are as follows:

$$F_{ei}^{\alpha\gamma}=-n_i\sum_{k,q}|u_{\alpha\gamma}(q)|^2 k_{\alpha x}\Pi_0^{\alpha\gamma}(k,q,\omega_{\alpha\gamma}) \ , \tag{B1}$$

$$F_{ep}^{\alpha\gamma}=-2\sum_{k,q,\lambda}|M_{\alpha\gamma}(q)|^2 k_{\alpha x}\Phi^{\alpha\gamma}(k,q,\omega_{\alpha\gamma}) \ , \tag{B2}$$

$$W_{ep}^{\alpha\gamma}=-2\sum_{k,q,\lambda}|M_{\alpha\gamma}(q)|^2 \varepsilon_{\alpha k}\Phi^{\alpha\gamma}(k,q,\omega_{\alpha\gamma}) \ , \tag{B3}$$

$$N_{ep}^{\alpha\gamma}=-2\sum_{k,q,\lambda}|M_{\alpha\gamma}(q)|^2 \Phi^{\alpha\gamma}(k,q,\omega_{\alpha\gamma}) \ , \tag{B4}$$

where

$$\Pi_0^{\alpha\gamma}(k,q,\omega_{\alpha\gamma})=2\pi[f(\xi_{\alpha k}/T_\alpha)-f(\xi_{\gamma,k+q}/T_\gamma)]\delta(\varepsilon'_{\alpha k}-\varepsilon'_{\gamma,k+q}-\omega_{\alpha\gamma}) \ , \tag{B5}$$

$$\begin{aligned}\Phi^{\alpha\gamma}(k,q,\omega_{\alpha\gamma})=&\Pi_0^{\alpha\gamma}(k,q,\omega_{\alpha\gamma}+\Omega_{q\lambda})[n(\Omega_{q\lambda}/T)-n(\xi_{\alpha k}/T_\alpha-\xi_{\gamma,k+q}/T_\gamma)]\\&+\Pi_0^{\alpha\gamma}(k,q,\omega_{\alpha\gamma}-\Omega_{q\lambda})[n(\Omega_{q\lambda}/T)-n(\xi_{\gamma,k+q}/T_\gamma-\xi_{\alpha k}/T_\alpha)] \ ,\end{aligned} \tag{B6}$$

with

$$\omega_{\alpha\gamma}=(\varepsilon_{\gamma,k+q}-\varepsilon_{\alpha k})-(\varepsilon'_{\gamma,k+q}-\varepsilon'_{\alpha k}) \ ,$$

$$f(\xi_{\alpha k}/T_\alpha)=1/\{\exp[(\varepsilon'_{\alpha k}-\mu_\alpha)/T_\alpha]+1\}$$

is the Fermi-Dirac distribution function, and

$$n(\Omega_{q\lambda}/T)=1/[\exp(\Omega_{q\lambda}/T)-1]$$

is the phonon occupation number. In Eqs. (B1)–(B6), all those terms with $\alpha=\gamma$ correspond to the intravalley scatterings due to impurities or phonons. The intraband Coulomb interaction can easily be included in our approach by using the random-phase approximation for the density-density correlation functions $\Pi_0^{\alpha\alpha}$, whose expressions are well known and will not be given here.

The Coulomb intervalley scattering results, F_{ee} and W_{ee}, are

$$F_{ee}^{\alpha\gamma}=\sum_q|v_c(q)|^2 q_x\int_{-\infty}^{\infty}\frac{d\omega}{\pi}\left[n\left(\frac{\omega}{T_\alpha}\right)-n\left(\frac{\omega+\omega_{\gamma\gamma}-\omega_{\alpha\alpha}}{T_\gamma}\right)\right]\Pi_2^{\alpha\alpha}(q,\omega)\Pi_2^{\gamma\gamma}(q,\omega+\omega_{\gamma\gamma}-\omega_{\alpha\alpha}) \ , \tag{B7}$$

$$W_{ee}^{\alpha\gamma}=\sum_q|v_c(q)|^2\int_{-\infty}^{\infty}\frac{d\omega}{\pi}\omega\left[n\left(\frac{\omega}{T_\alpha}\right)-n\left(\frac{\omega+\omega_{\gamma\gamma}-\omega_{\alpha\alpha}}{T_\gamma}\right)\right]\Pi_2^{\alpha\alpha}(q,\omega)\Pi_2^{\gamma\gamma}(q,\omega+\omega_{\gamma\gamma}-\omega_{\alpha\alpha}) \ , \tag{B8}$$

where $\Pi_2^{\alpha\alpha}(q,\omega)$ is the imaginary part of the electron density-density Green's functions for the αth valley, in which the electron-electron interaction has been considered under the random-phase approximation.[18]

APPENDIX C: THE EXPRESSIONS OF $1/\tau$ AND n_{c_∞} IN EQ. (44)

For the case of the electrons in quasiequilibrium which obey the Maxwell-Boltzmann distribution, we have

$$n_\alpha=\sum_k f(\xi_{\alpha k}/T_\alpha)/N=\sum_k\exp[-(\xi_{\alpha k}-\mu_\alpha)/T_\alpha]/N \ , \tag{C1}$$

or

$$\exp(\mu_\alpha/T_\alpha)=(Nn_\alpha/2)(2\pi/m_D T_\alpha)^{3/2} \ , \tag{C2}$$

where α stands for the αth valley. When the electric field is applied along the $\langle 100\rangle$ direction, we have two cold val-

leys ($\alpha=c$) and four hot valleys ($\alpha=h$), and $n_c=(1-4n_h)/2$. Due to Eqs. (C1) and (C2), Eqs. (B5) and (B6) in Appendix B take simpler forms:

$$\Pi_0^{ch}(k,q,\omega_{ch})=\pi N(2\pi/m_D)^{3/2}(n_c H_{ck}-n_h H_{h,k+q})\delta(\varepsilon_{ck}-\varepsilon_{h,k+q}) , \tag{C3}$$

and

$$\begin{aligned}\phi^{ch}(k,q,\omega_{ch})=\pi N(2\pi/m_D)^{3/2}\{&[n_c H_{ck} n(\Omega_{q\lambda}/T)+n_h H_{h,k+q} n(-\Omega_{q\lambda}/T)]\delta(\varepsilon_{ck}-\varepsilon_{h,k+q}+\Omega_{q\lambda})\\ &-[n_c H_{ck} n(-\Omega_{q\lambda}/T)+n_h H_{h,k+q} n(\Omega_{q\lambda}/T)]\delta(\varepsilon_{ck}-\varepsilon_{h,k+q}-\Omega_{q\lambda})\} ,\end{aligned} \tag{C4}$$

where

$$H_{\alpha k}=\exp(-\xi_{\alpha k}/T_\alpha)/T_\alpha^{3/2} \quad (\alpha=c,h), \quad n_h=(1-2n_c)/4 . \tag{C5}$$

Substituting (C4) into (B4) and (43), and comparing them with Eq. (44), we get

$$\begin{aligned}1/\tau=&4\pi(2\pi/m_D)^{3/2}\\ &\times\sum_{k,q,\lambda}|M_{ch}(q,\lambda)|^2\{[H_{ck} n(\Omega_{q\lambda}/T)-0.5H_{h,k+q} n(-\Omega_{q\lambda}/T)]\delta(\varepsilon_{ck}-\varepsilon_{h,k+q}+\Omega_{q\lambda})\\ &-[H_{ck} n(-\Omega_{q\lambda}/T)-0.5H_{h,k+q} n(\Omega_{q\lambda}/T)]\delta(\varepsilon_{ck}-\varepsilon_{h,k+q}-\Omega_{q\lambda})\} ,\end{aligned} \tag{C6}$$

and

$$\begin{aligned}n_{c\infty}/\tau=&-\pi(2\pi/m_D)^{3/2}\sum_{k,q,\lambda}|M_{ch}(q)|^2 H_{h,k+q}\\ &\times[n(-\Omega_{q\lambda}/T)\delta(\epsilon_{ck}-\epsilon_{h,k+q}+\Omega_{q\lambda})-n(\Omega_{q\lambda}/T)\delta(\epsilon_{ck}-\epsilon_{h,k+q}-\Omega_{q\lambda})] .\end{aligned} \tag{C7}$$

It can be shown that $1/\tau$ will decrease rapidly with decreasing lattice temperature T. As $T\to 0$, $1/\tau$ vanishes, which corresponds to the case where there is no repopulation effect.

---

*On leave from the Department of Physics, Nanjing Institute of Technology and Nanjing University, Nanjing, China.

[1]E. M. Conwell, *High Field Transport in Semiconductors* (Academic, New York, 1967).
[2]K. Seeger, *Semiconductor Physics* (Springer-Verlag, Berlin, 1982).
[3]L. Reggiani, *Hot-Electron Transport in Semiconductors* (Springer-Verlag, Berlin, 1985).
[4]C. Canali, C. Jacoboni, F. Nava, G. Ottaviani, and A. Alberigi-Quaranta, Phys. Rev. B **12**, 2265 (1975).
[5]M. A. Littlejohn, J. R. Hauser, and T. H. Glisson, J. Appl. Phys. **48**, 4587 (1977).
[6]M. H. Jorgensen, Phys. Rev. B **18**, 5657 (1978).
[7]M. Asche, Z. S. Gribnikov, V. M. Ivatshchenko, H. Kostial, and V. V. Mitin, Phys. Status Solidi B **114**, 429 (1982).
[8]C. J. Stanton, H. U. Baranger, and J. W. Wilkins, Appl. Phys. Lett. **49**, 176 (1986).
[9]D. N. Zubarev, *Nonequilibrium Statistical Thermodynamics* (Consultants Bureau, New York, 1974).
[10]V. P. Kalashnikov, Physica (Utretcht) **48**, 93 (1970).
[11]D. Y. Xing, P. Hu, and C. S. Ting, Phys. Rev. B **35**, 6379 (1987).
[12]D. Y. Xing, and C. S. Ting, Phys. Rev. B **35**, 3971 (1987).
[13]B. G. Bosch and R. W. H. Englemann, *Gunn-Effect Electronics* (Wiley, New York, 1975).
[14]X. L. Lei, D. Y. Xing, M. Liu, C. S. Ting, and J. L. Birman, Phys. Rev. B **36**, 9134 (1987).
[15]X. L. Lei and C. S. Ting, Phys. Rev. B **32**, 1112 (1985).
[16]H. Mori, Prog. Theor. Phys. **33**, 423 (1965).
[17]R. Zwanzig, J. Chem. Phys. **40**, 2527 (1964).
[18]X. L. Lei and C. S. Ting, Phys. Rev. B **30**, 4809 (1984).
[19]J. M. Ziman, *Principle of the Theory of Solids* (Cambridge University Press, London, 1972).
[20]P. N. Argyres and J. L. Sigel, Phys. Rev. B **9**, 3197 (1974).
[21]M. Huberman and G. V. Chester, Adv. Phys. **24**, 489 (1976).
[22]R. Kubo, Can. J. Phys. **34**, 1274 (1956).
[23]W. Y. Lai and C. S. Ting, Phys. Rev. B **24**, 7206 (1981).
[24]N. G. Van Kampen, Phys. Norv. **5**, 10 (1971).
[25]N. J. M. Horing, X. L. Lei, and H. L. Cui, Phys. Rev. B **33**, 6929 (1986).
[26]C. Herring and E. Vogt, Phys. Rev. **101**, 944 (1956).
[27]H. W. Streitwolf, Phys. Status Solidi **37**, K47 (1970).
[28]M. Lax and J. L. Birman, Phys. Status Solidi B **49**, K153 (1972).
[29]X. L. Lei and C. S. Ting, Phys. Rev. B **36**, 8162 (1987).